ICAS 2016
30th Congress of the International Council of the Aeronautical Sciences
DCC, Daejeon, Korea ; September 25-30, 2016

STAGGERED THREE-DIMENSIONAL CAVITIES AS A POSSIBLE METHOD FOR SKIN FRICTION DRAG REDUCTION

E. R. Gowree* and C. J. Atkin*
***Department of Mechanical Engineering and Aeronautics, City University London**

Abstract

The effect of three-dimensional staggered circular cavities on a zero-pressure gradient incompressible turbulent boundary layer was studied. Two key parameters were varied, being the ratio of the diameter, d, to the depth, h, of the cavity, d/h and the Reynolds number based on the diameter of the cavity, R_d. Velocity profile measurements showed that for the cases of d/h>1 an increase in skin friction drag was experienced with respect to a smooth surface, but for d/h ≤ 1 the drag increment was almost negligible and in some cases it was lower than that of a smooth surface by up to 10%. Measurements along the spanwise plane showed the presence of organised transverse velocity components which bear some resemblance with the flow over riblets. The skin friction drag appears to be a strong function of R_d, where for R_d >5500 a drag increment is experienced which could potentially be due to shear layer breakdown and more production of turbulence.

1 Introduction

It is an established fact that surface roughness or other excrescences such as grooves and cavities are major sources of skin friction drag penalty from turbulent boundary layers in wall bounded flows. These findings were supported by the pioneering studies of Nikuradse [1] who also derived the initial semi-empirical relations which could assist in estimating the drag increment with respect to a hydrodynamically smooth surface. Since then a vast amount of research has been conducted which supports Nikuradse's findings and also provides further insight into the physical mechanism improving the initial semi-empirical and numerical models and a very detailed review was presented by Jimenez [2]. A new perspective was introduced by Walsh [3] in the 1980s by demonstrating that grooves aligned with the streamwise direction, if sufficiently submerged in the viscous sub-layer, could help in reducing the viscous drag by almost 10%. More experimental validation was provided by Choi [4] in the late 1980s including details of the physical mechanism behind riblet control and further studies followed, by Berchert and co-workers [5], [6] and [7], over a period a more than two decades using highly viscous fluid to assist in resolving the flow structures.

In a reversal of bio-inspired thinking it was thought that, if the riblet mechanism was effective then nature would have got there first and this triggered the idea that the mechanism might already be present on the skin of fast swimming sharks. Recent studies by Dean and Bhushan [8] focused on measurements on surfaces emulating the texture of shark skin together with the addition of mucus within the grooves. They postulated that the mucus presents an added benefit and therefore, coupled with super-hydrophobic material, the performance of riblets could be further improved. Further insight in the physical process through which the drag reduction occurs was provided analytically by Luchini et al. [9]. Following Karniadakis and Choi [10], in simple terms riblets acts as fences aligned along the streamwise direction which hinder the spanwise propagation of the coherent longitudinal structures during the 'sweep' event, where the high momentum fluid moves towards the wall as a result of turbulent mixing. Whereas during the 'burst' event the fluid drawn away from the wall has lower momentum. Therefore, reducing the stretching of the longitudinal vortices would lead to increased momentum upwash from the

wall during the 'burst' event, which in turn reduces the wall shear stress.

Most of these studies have dwelled mainly on riblets, however Tani [10] suggested that randomly distributed roughness could also lead to similar drag reduction benefit without explaining the mechanism in detail. Later, Sirovich and Karlsson [11] demonstrated that a staggered array of discrete protrusions with a 'V' shaped cross-section could also reduce skin fiction drag, whereas the aligned protrusions led to drag increment. They postulated that the physical mechanism responsible for drag reduction was completely different to that of riblets but could be similar to the mechanism that exists during spanwise wall oscillation, where the normal process of the turbulent energy production is reversed as the longitudinal vortices creates a high momentum upwash and lower momentum downwash. Based on the plane wave propagation analogy of Sirovich et al. [13], where the coherent streamwise structures, referred as 'rolls' and which are the energy bearing modes, interact with the propagating oblique modes leading to turbulent energy production through the events of 'burst' and 'sweep'. The most influential obliquely propagating modes are oriented by 45 to 65 degrees, Sirovich and Karlsson demonstrated that, by modifying the phase of the propagating oblique waves, the energy production could be reduced resulting in a drag reduction from their randomly staggered array of protrusions.

The current investigation was focused on studying the effect of staggered discrete circular cavities in a zero pressure gradient turbulent boundary layer and to explore any correlation between the modifications of the coherent structures in the flow with measured friction drag reduction. Similar to the case of riblet or spanwise wall oscillation, the intention of staggering the cavities was to re-organise the transverse velocity components which have been shown in previous work to hamper the production of turbulent energy.
Hot wire anemometry (HWA) was used to capture the velocity profile very close to the wall, with reasonable accuracy using the optical alignment technique developed by Gowree et al. [14]. Further measurements were made using three component Laser Doppler Anemometry (LDA) to capture the three dimensional flow field in the spanwise plane so as to understand the physical mechanism for the drag reduction.

2 Experimental Arrangements

The experiment was conducted in the T2 low speed wind tunnel at the Handley Page laboratory at City University London, which has a working section of *0.8m* by *1.12m* by *1.8m*. The experimental model was a wooden flat plate with an elliptical leading edge of a ratio of *5:1*, it is also equipped with a trailing edge flap to adjust the location of the stagnation point and to approach a zero pressure gradient condition within the experimental domain. The initial laminar boundary layer was tripped using a *0.2mm* trip-wire placed at 100mm downstream of the leading edge and its effectiveness in generating a turbulent boundary layer was confirmed by the hot wire signal. A streamwise row of surface pressure tappings, offset by *100mm* from the tunnel centreline, was used to check the pressure gradient. The dimensions of the plate are shown in Fig. 1, together with the *192×192mm* perforated acrylic panel where the thickness or depth, h, and spacing, s, were kept constant at 3mm and 20mm respectively and the diameter of the cavity, d, varied between 2 to 5mm. Fig. 1 also shows the surface mounted, single axis traverse system used to capture the velocity profiles of the boundary layer using hot wire anemometry.

King's law was applied for the hot wire calibration and the velocity profile was captured using the surface mounted traverse which has a resolution of 5μm per step, together with the digital-optical system developed by Gowree et al. [14], to position the hot wire accurately as close as possible to the wall. The combination of this particular traverse system and the optical alignment system has been shown to capture the flow very close to the wall which is crucial for

accurate calculation of boundary layer integral quantities. As the traverse system had to be permanently fixed to the surface of the model, the hot wire traverse was limited to a single location along the centreline of the model and downstream of the final row of the cavities.

For more detailed flow diagnosis three component LDA measurements was performed using a tri-axis traverse system which assisted in the measurement of a larger spatial domain as opposed to the hot wire. The DANTEC Dynamics LDA system was used while operating in backward scatter mode. Based on the focal length of the lenses a probe volume of approximately $120\times120\times2600\mu m$ was obtained. In order to measure as close as possible to the wall the two component laser head was rotated by 45˚ so that the two opposite beams were along the horizontal axis and was tilted by about 3˚ to account for beam expansion. The use of 800mm lenses led to a compromise in the spatial resolution in which case the hot wire technique could be considered superior, but still it was limited to a single component measurement and this benefit would even out with a multiple component probe. Therefore, the hot wire measurement was focussed on resolving the turbulent velocity profiles accurately and the LDA to capture the transverse spatial structures in the flow downstream of the cavities at the same streamwise position as the hot wire measurements. Surface oil flow visualisation was also performed to obtain a qualitative understanding of the flow physics in the vicinity and downstream of the cavities. The experiment was conducted with the perforations (a) sealed on the reverse side of the acrylic sheets, as shown on the bottom right of Fig. 1, and (b) open to a single plenum underneath the perforated panel.

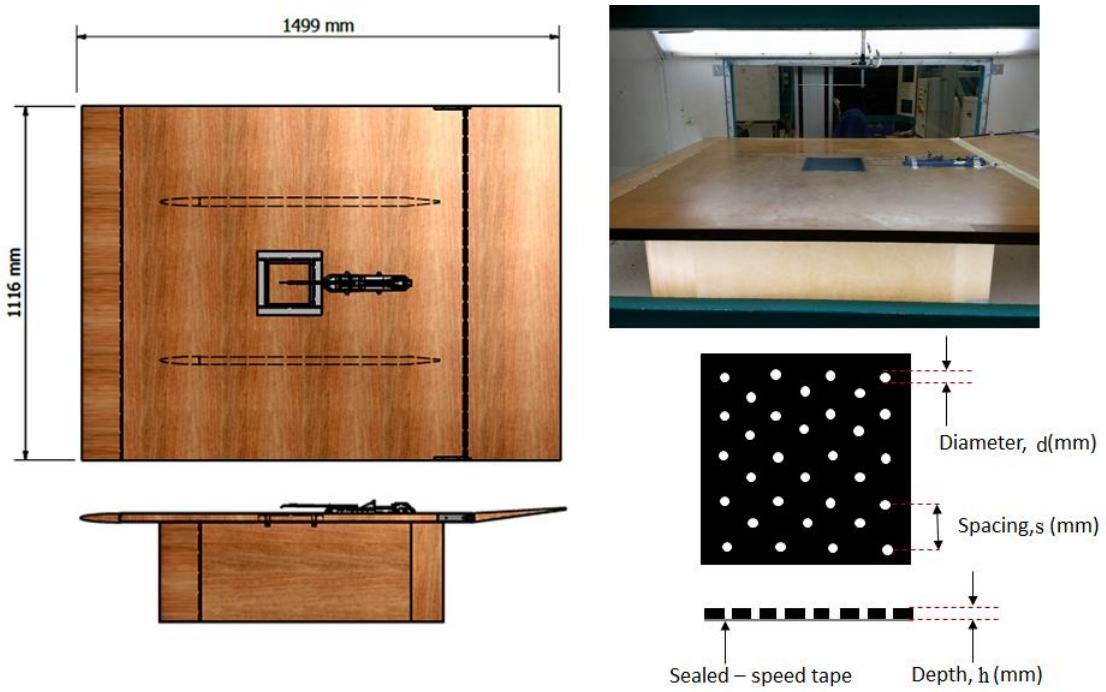

Fig. 1: The top and side view of the flat plate (left) and the plate mounted in test section of the wind tunnel (top right).

3 Results

3.1 Unperforated Plate

The desired zero pressure gradient condition within the experimental domain was confirmed from Fig. 2 which shows the velocity gradient in the streamwise direction. This also assisted in the selection of the streamwise position for the velocity profile measurements, which was located at *730mm* downstream of the leading edge. The initial hot wire traverse was made on the baseline smooth unperforated panel for later comparison with the results from the perforated cases. From the velocity profiles captured on the smooth surface the skin friction was determined using Clauser's chart technique [3], where the 'inner layer' logarithmic region law was defined by a Karman constant of *0.4* and y-intercept of *5.1*.

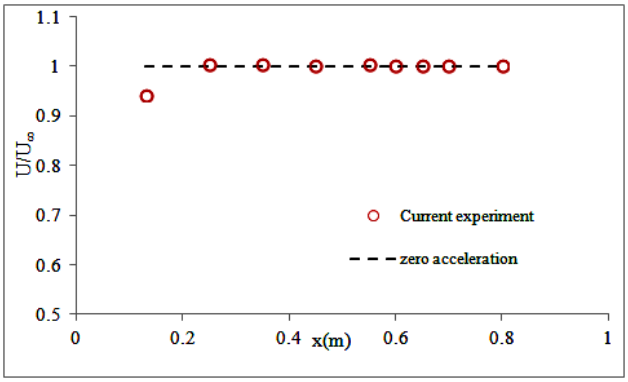

Fig. 2: The streamwise velocity gradient along the flat plate.

The resulting shear stress was used to express the velocity profiles in wall units as shown in Fig. 3 where a good agreement can be observed with the linear region of the inner layer. From the velocity profiles the boundary layer integral quantities was calculated and the skin friction coefficient was expressed as a function of the Reynolds number based on the momentum thickness, θ, as shown in Fig. 5. The results from the smooth case can be compared with the semi-empirical relation given by Gaudet [16] and the DNS results from Jimenez et al. [17]. At lower R_θ the current experimental results show closer agreement with the DNS results; however, throughout the whole range of R_θ tested, the agreement was within *2%* of Gaudet's results.

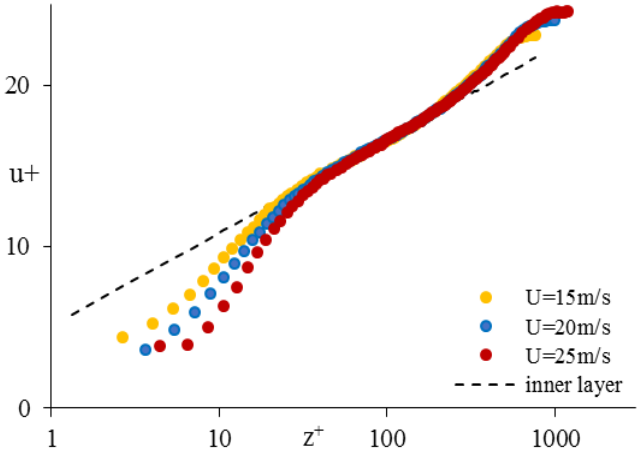

Fig. 3: Velocity profiles along unperforated plate at x=730mm. The inner layer is defined by $z^+ = 2.5\ ln\ u^+ + 5.1$.

3.2 Effect of 3D Cavities on the Mean Flow

The local skin friction from the perforated panel was determined using Clauser chart technique, for the same von Karman constant and y-intercept used for the unperforated cases. The results are presented in Fig. 5 and were also used to express the velocity profiles in wall units which can be compared against the smooth unperforated case in Fig. 4, for a freestream velocity of *15m/s* and the cavities sealed at the bottom. For cavities of $d>3mm$, the downward shift in the linear inner layer in Fig. 4 shows an increase in the local skin friction similar to the behaviour noticed in turbulent boundary layer over rough walls. This behaviour is in line with the observations of Nikuradse [2] and Clauser [1] and many others summarised by Jimenez [3]. However, the upward shift in the inner layer for the cases where $d\leq3$ suggests that a reduction in local skin friction is encountered. This observation is clearer in Fig. 5 which summarises the skin friction coefficient from all the surfaces tested with the bottom both sealed and opened. The difference between results from the cavities being sealed and open is small

and could be influenced by experimental uncertainty.

From dimensional analysis, the ratio d/h and the Reynolds number based on the diameter of the cavity, R_d, were considered to the influential geometrical parameters and the skin friction obtained from Clauser technique was plotted against these dimensionless groups in Fig. 6 for freestream velocity of 15, 20 and 25m/s. From the left hand side of Fig. 6 a well-defined trend is present, suggesting that for d/h ≤ 1, a drag reduction as much as approximately 10% could be obtained, and for d/h > 1 there is a sharp drag rise and for the cases studied this could amount to 10% as well. However, from the right hand side of Fig. 6, the effect of Reynolds number is rather ill-defined, except in the cases where d ≤ 3mm where the skin friction benefit is slightly reduced with increasing R_d.

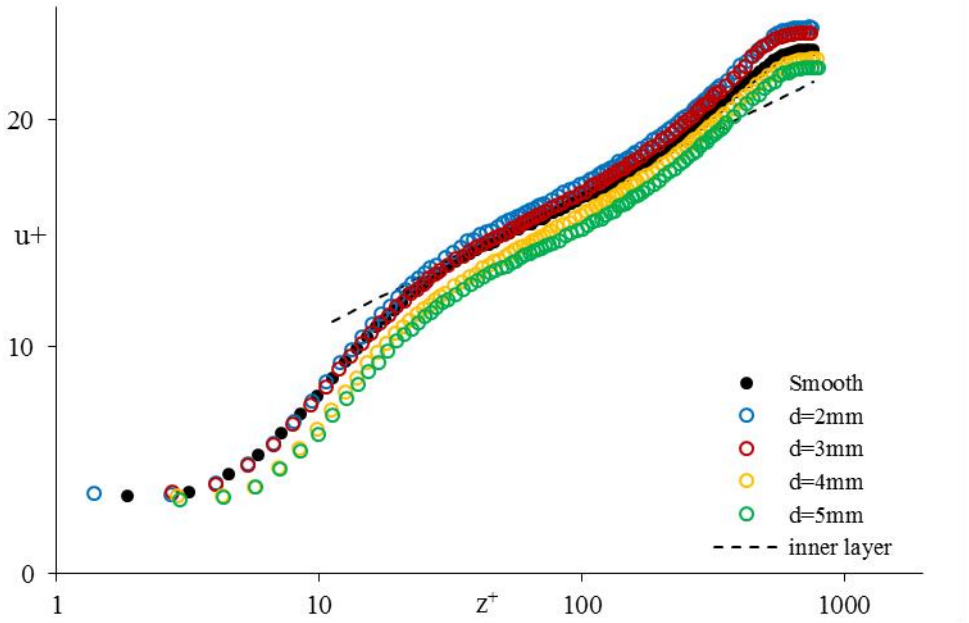

Fig. 4: Velocity profiles along perforated plates at x=730mm and the bottom of the cavity sealed.

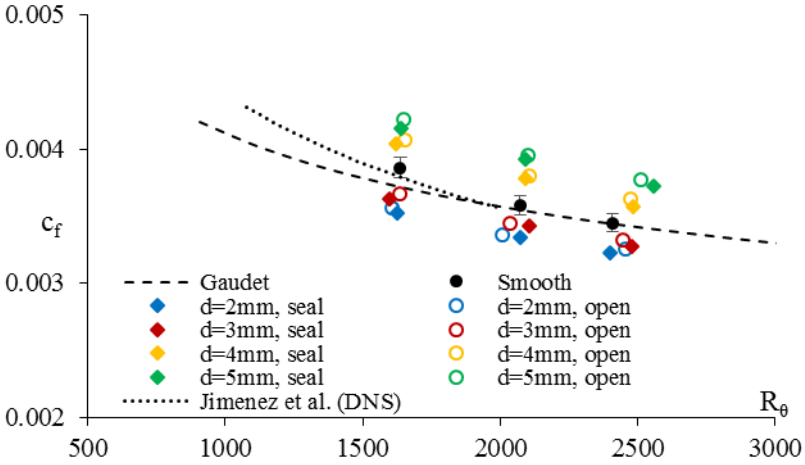

Fig. 5: The local skin friction on the different of surfaces tested, where the baseline smooth case is compared with the DNS study of Jimenez [7] and the semi-empirical relation given by Gaudet [8].

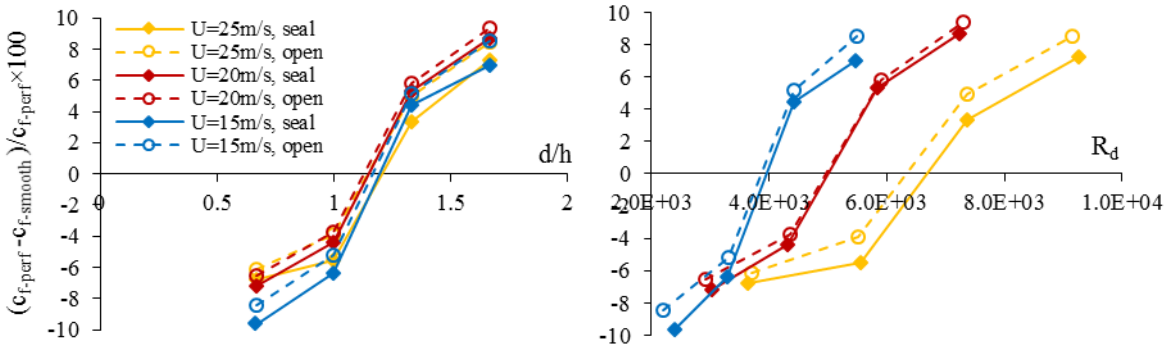

Fig. 6: The percentage difference in skin friction between the perforated and smooth cases as a function of the ratio, d/h (left) and R_d (right).

For a zero pressure gradient flow, the momentum integral equation can be reduced to

$$\frac{d\theta}{dx} = \frac{c_f}{2} \qquad (1)$$

The effect of the cavities on the turbulent boundary layer can be further analysed by considering the momentum thickness, θ, whereby for a zero pressure gradient flow the local skin friction is directly proportional to the rate of change of momentum deficit as given by Eq. 1. The trend in the momentum thickness has been presented in Fig. 7. An increase in Δθ is observed from Fig. 7 (left) with increasing d/h and this behaviour is to be expected since c_f is directly proportional to θ, but the rate of change is less steep compared to that on the left of Fig. 6. Moreover, for the lowest speed tested, U=15m/s, a reduction in θ can be observed for all the ratios of d/h tested and it appears that θ is more strongly correlated to Reynolds number rather than d/h. This observation contradicts the trend from Fig. 5 and Fig. 6, where a skin friction penalty was observed for the cases of d > 3mm. Similarly, from the figure on the right a negative Δθ is observed for all the cavities tested at a freestream velocity of 15m/s. The relation between θ and R_d is well-defined and there seem to exist a critical regime at R_d < 6000 where the skin friction reduction is observed.

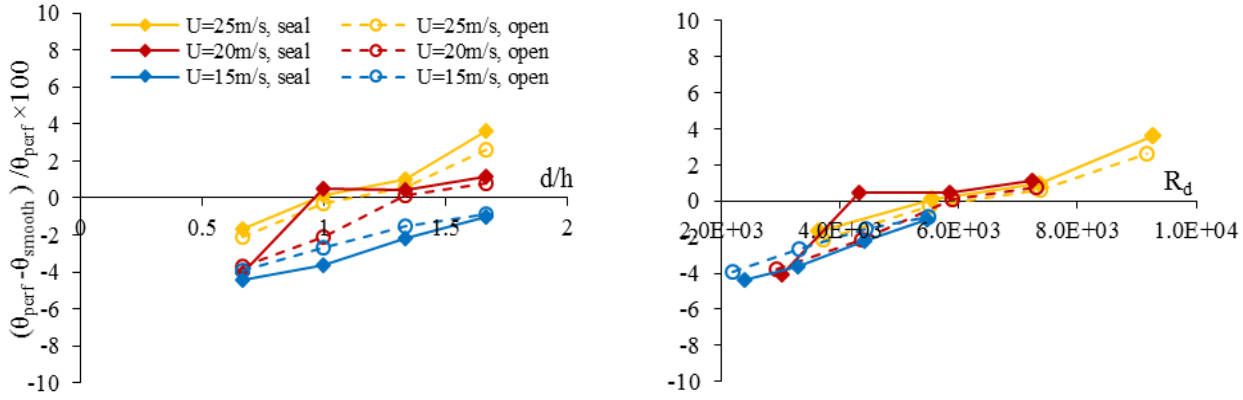

Fig. 7: The percentage difference in momentum thickness between the perforated and smooth cases as a function of the ratio, d/h (left) and R_D (right)

3.3 Topology of Surface Streamlines

The surface streamline patterns in the vicinity and downstream of the cavities are shown below in Fig. 8 which was obtained using oil flow visualisation for the 3mm and 5mm cavity at 15, 20 and 25m/s respectively from top to bottom. The circular cavities promote the formation of vortical structures and at velocity of 20 and 25 m/s, they impinge directly on the downstream cavities as shown in the bottom two figures on the right for the case of 5mm cavities. These vortices could potentially be in the form of a primary hairpin vortices commonly found during surface blowing or suction however with limited experimental data it is too early to confirm whether they are hairpin or horseshoe type. The main difference between them being, if viewed from the trailing edge the left 'leg' of the hair pin vortex will rotate in the clockwise direction and the right 'leg' in the counterclockwise direction and the horseshoe vortex will be completely opposite. For the cases shown in the first row, a drag reduction was experienced, where in the 3mm case (top left) the reattachment region was smaller than the 5mm case (top right). Also, in the 3mm case at 15m/s, the vortical structures introduce a lateral velocity component which is clearer from the surface streamline pattern and also present at 20 m/s (middle left). Note that in both cases a reduction in c_f was observed. The effect is not very clear at 25m/s in the bottom left figure, where the drag difference with respect to the clean surface was positive and very small.

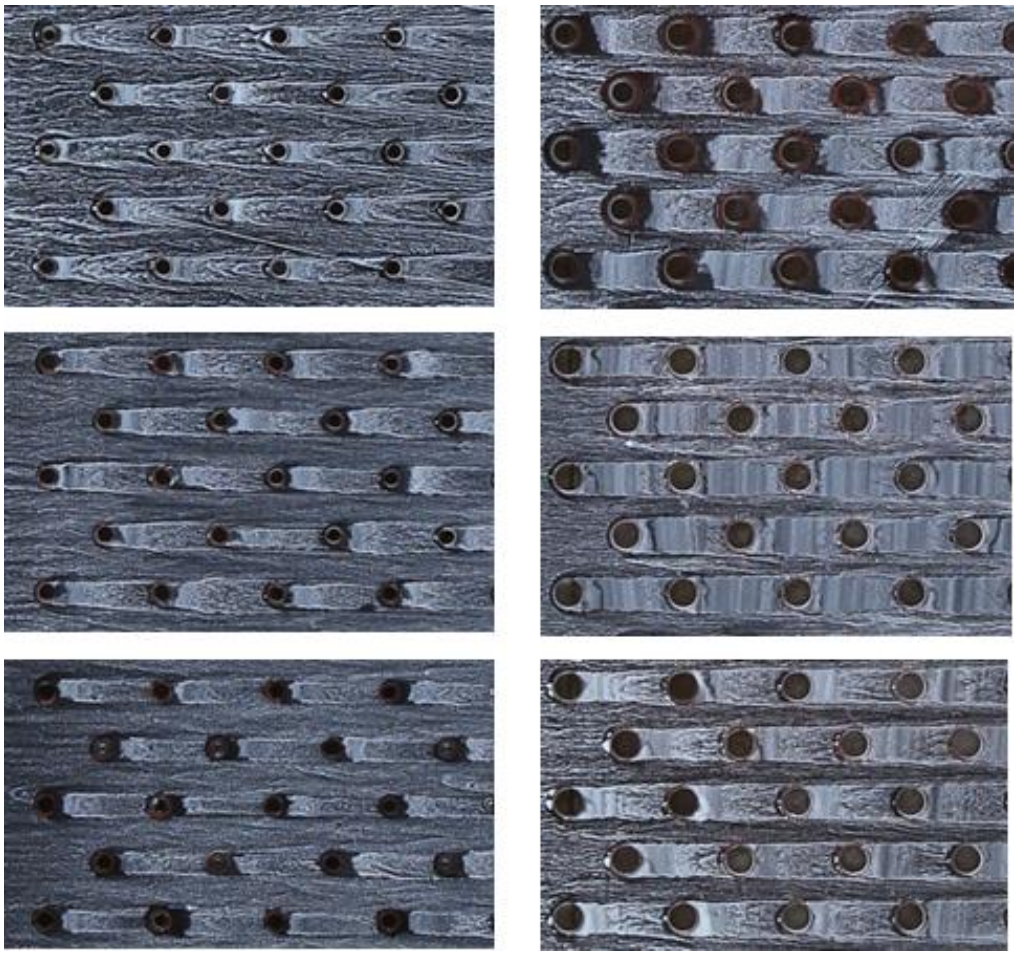

Fig. 8: Surface streamline visualisation of the flow around the circular cavity of d=3mm (left) and d=5mm (right). Where the freestream velocity from top to bottom are from 15, 20, 25m/s respectively.

3.3 The 3D Flow Field along the Span

The three-dimensional flow field captured using the LDA technique is presented in this section. The data was filtered based on the validation levels where all measurements below a level of *30%* was discarded. A spline fit algorithm was employed to interpolate the contours and this resulted in a more organised representation of the turbulence structures. All the measurements were made in the plane bounded by the transverse and wall normal axes, *y* and *z* respectively, at *x=730mm* which was approximately *10mm* downstream of the last row of cavities as shown in Fig. 9. The centreline of the plate corresponds to *y=0* which was also the centreline of the middle row of holes. The normalised mean streamwise, u/U_e, and spanwise velocity components, w/U_e, are shown in Fig. 10 for the cases of d=3mm on the left and d=5mm on the right. Note that at this freestream velocity, U_∞ *=20m/s*, for *d=3mm*, a drag reduction was encountered whereas for *d=5mm*, the drag increased in comparison to a smooth surface. From the normalised mean streamwise velocity components shown at the top of Fig. 10, near the wall a region of lower momentum can observed at *y=±5mm*. This region is in between the primary vortex pairs generated by two adjacent cavities. However, these pockets of low streamwise momentum fluid are induced by the vortex legs of the counter-rotating vortex pair and suggest that the direction of rotation is away from the centre plane similar to a hairpin vortex mentioned above. This could be a potential explanation of the wedge-like surface streamline seen from Fig. 8. The high transverse momentum region along the centreline of the cavities is a result of lateral shearing in the region bounded by the vortex pair. This feature is not that obvious for the case of *d=5mm*, shown on the right of Fig. 10, but in both cases the presence of large transverse component creates a diving region between the low momentum fluid closer to the wall and the high momentum fluid above.

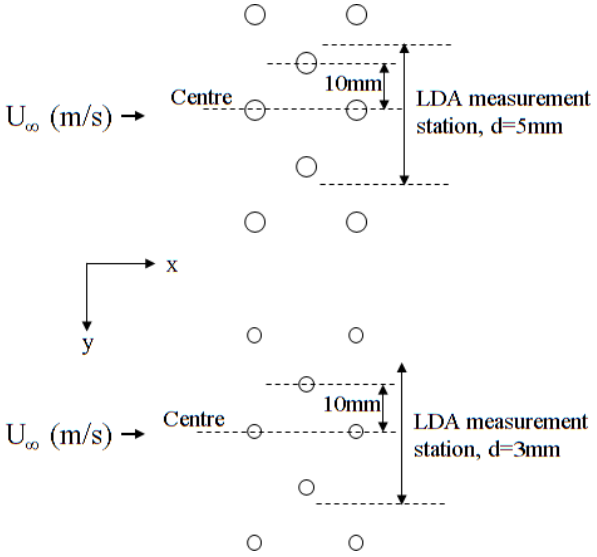

Fig. 9: Schematic representation of the top-view of the LDA measurement station.

The rms of the fluctuating streamwise, u'/U_e, and transverse velocity component, v'/U_e, (normalised by the mean streamwise velocity component at the edge of the boundary layer) are shown at the top and bottom of Fig. 11 respectively, for *d=3mm* (left) and *d=5mm* (right). Considering the case of *d=3mm*, the high streamwise velocity fluctuations along *y=0* are expected as this region is bound by the vortex which enhances turbulence mixing, similarly at *y=±10mm*. The pocket of low mean streamwise velocity at *y=±5mm* observed from Fig. 10 is accompanied by low velocity fluctuations as shown on the top right of Fig. 11. This reduction in streamwise velocity fluctuation towards the centre of this region indicates the presence of a vortex core and hence a secondary vortical flow in the region clear of any holes which lies between the legs of two adjacent vortices. From the bottom left of Fig. 11, this particular spanwise position also possesses very low transverse velocity fluctuations, but it is followed by a dividing region at *z≈2mm* where two concentrated regions of even higher transverse velocity fluctuations are present exactly in the same location as the low streamwise velocity fluctuations near the wall. For the case of *d=5mm*, the low velocity fluctuation was not present at *y=±5mm* but the overall magnitude of the fluctuating streamwise components near the

wall was larger and also the intensity of the transverse component in the dividing region.

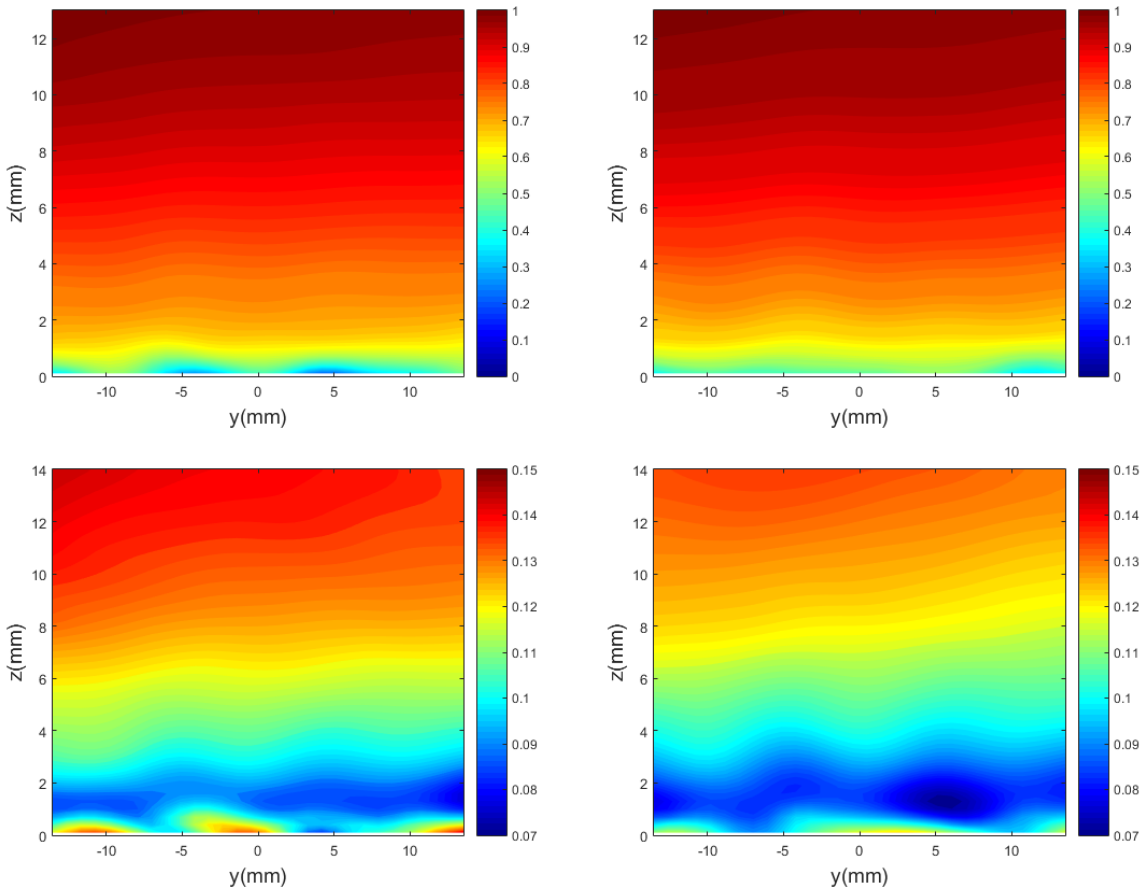

Fig. 10: The normalised mean streamwise, u/U_e top and transverse v/U_e (bottom) velocity components for the d=3mm (left) and d=5mm (right).

4 Discussion

The skin friction measured for the baseline smooth case agrees well with the universal 'log-law' in Fig. 3, the skin friction results obtained from DNS and semi-empirical results, providing confidence in the measurement technique and the data analysis process. From Fig. 4 the upward shift of the inner layer for the cases where $d > 3\ mm$ suggests that the local skin friction is reduced, an observation not reported previously. Small differences in skin friction between the opened and sealed cavities are thought to be due to the low levels of pressure fluctuation and thus weak forcing of the flow into the plenum under the perforated sheet. Larger magnitude of flow transpiration would be expected to lead to large skin friction increments which were clearly not observed in the present work. Using the Clauser chart technique, a skin friction reduction was observed for a ratio of cavity diameter to height ratio, $d/h<1$, but a different trend was obtained from the momentum thickness results. The point to be noted is that the Clauser chart technique might be restricted to cases where the von Karman constant from the universal logarithmic does not differ from that of an equivalent smooth wall. The trend in the momentum thickness from Fig. 7 was slightly more conclusive where, it was found to be a stronger function of the Reynolds number based on the diameter, R_d rather than d/h. There seem to be a critical regime where the drag reduction benefit disappears at $R_d > 5500$.

Surface flow visualisation shown in Fig. 8 helped in shedding some light on the three-

dimensional flow field, where some features of the vortical structures generated by cavities were captured. These revealed the spanwise non-uniformity of the flow and the presence of transverse velocity components. Bearing this in mind the spanwise variation of the local skin friction was checked by expressing the velocity profiles from the LDA measurements on a Clauser chart. But not presented in this paper. Hot wire measurements at different spanwise positions would have been preferable due to the higher accuracy in capturing the velocity profiles but unfortunately the surface mounted traverse had to be permanently fixed at one particular position. The velocity profiles captured from the LDA suffered from poor near-wall resolution and therefore were deemed unsuitable for determining the momentum thickness. However, when presented on a Clauser chart, both an upward and downward shift in the linear region was observed between the profiles at each spanwise station, around a mean profile close to the velocity profile along the centreline. This provides additional support to the idea that the drag reduction is not just a localised benefit observable in the momentum deficit region in the wake of the trailing vortex. Also, from Fig. 8, larger momentum deficit would be expected for the case of *d=5mm*, where the wake is more clearly defined: conversely these cases were found to have higher skin friction drag.

The LDA measurements were useful in capturing the turbulent structures which helped in generating some insight into the possible mechanism of drag reduction and also understanding the vortical structures which left a footprint on the surface streamlines shown in Fig. 8. The primary vortex pair generated at each cavity could potentially be of hairpin type. As shown on the left of Fig. 10 and Fig. 11, for the case *of d=3mm* where a skin friction reduction was observed, a secondary vortical flow was observed. This secondary vortex resides in between the legs of two adjacent vortex pairs. Referring back to Section 1, in previous studies skin friction reduction had been achieved by manipulating the transverse velocity component either using riblets, spanwise oscillation or randomly distributed protrusions. According to Berchert et al. [6], a reduction in the fluctuating transverse or spanwise velocity component near the wall will result in a reduction in turbulent energy production and hence lower shear stress. With the current limited results one could only speculate that the reduced transverse velocity fluctuations at $y=\pm 5mm$ for the *d=3mm* case could be a contributing factor to the observed skin friction reduction, unlike in the *d=5mm* case. For *d=3mm* both the mean and fluctuating transverse velocity component are organised in a similar fashion to that of the flow over riblets, suggesting that the drag reduction mechanism could be similar. However, the scenario present in the case studied by Sirovich and Karlsson is yet to be ruled out.

Despite the presence of larger magnitudes of the transverse velocity components, which seems to be main contributing factor for drag reduction, this was not the case for d=5mm, except for freestream velocity, $U_\infty > 15m/s$. Here, the flow structures are organised in such a way that, downstream of the first couple of rows of cavities, the primary vortices break down and merge into a shear layer with large associated transverse velocity fluctuations, as seen in the bottom right of Fig. 11. This could explain the Reynolds number dependence observed on the left of Fig. 7, where a shear layer instability affects the structure of the transverse velocity component responsible for the drag reduction.

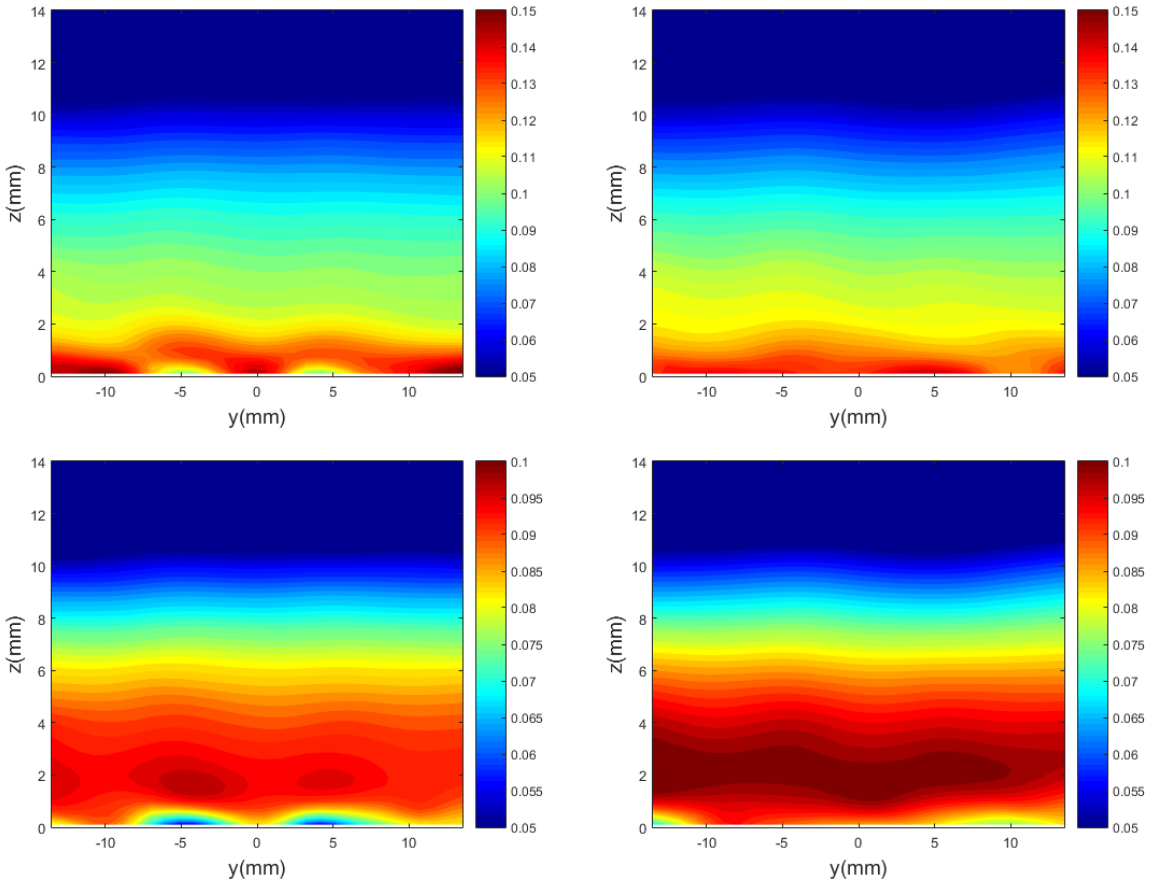

Fig. 11: The normalised rms streamwise velocity, u'/U_e (top) and transverse v'/U_e (bottom) velocity components for the d=3mm (left) and d=5mm (right).

5 Conclusion

This set of initial results have suggested that, similar to riblets, staggered three-dimensional cavities could be a potential passive method for skin friction drag reduction. Following a parametric study, the drag benefit was observed to be limited to some extent to the ratio of *d/h* and but a strong function of the Reynolds number based on diameter of the cavity, R_d. Surface flow visualisation showed the presence of a primary vortical structure generated by the cavity. Further LDA measurements along a spanwise plane for *d=3mm* showed the presence of a secondary vortex between the legs of two adjacent primary vortices which organises the transverse fluctuating velocity in a similar fashion to the flow in the presence of riblets. The main benefit of staggered cavities is the lower excrescence drag penalty in comparison to that from riblets.

References

[1] J. Nikuradse, "Stromungsgesetze in rauhen Rohren," VDI-Forsch; VDI-Verlag, Berlin, 1933.

[2] J. Jimenez, "Turbulent Flows over Rough Walls," *Annual Reviews of Fluid Mechanics*, 2004.

[3] M. J. Walsh, "Drag Characteristics of V-groove and transverse curvature riblets," *Progress in Astronautics and Aeronautics*, vol. 72, pp. 168-184, 1980.

[4] K. S. Choi, "Near-wall structure of a turbulent boundary layer with riblets," *Journal of fluid mechanics*, vol. 209, pp. 417-458, 1989.

[5] D. W. Berchert and M. Bartenwerfer, "The viscous flow on surfaces with longitudinal ribs," *Journal of fluid mechanics*, vol. 206, pp. 105-129, 1989.

[6] D. W. Berchert, M. Bruse, H. W., J. G. T. van der Hoeven and G. Hoppe, "Experiments on drag reducing surfaces and their optimisation with an adjustable geometry," *Journal of fluid mechanics*, vol. 338, pp. 59-87, 1997.

[7] D. W. Berchert, M. Bruse and W. Hage, "Experiment on Three-Dimensional Riblets as an Idealised Model

of Shark Skin," *Experiments in Fluids*, vol. 28, p. 403, 2000.

[8] B. Dean and B. Bhushan, "Shark-skin surfaces for flui-drag reductio n in turbulent flow: a revies," *Philosophical Transaction of the Royal Society, A*, vol. 368, pp. 4775-4806, 2010.

[9] P. Luchini, F. Manzo and A. Pozzi, "Resistance of a grooved surface computed to parallel flow and crossflow," *Journal of fluid mechanics*, vol. 228, pp. 87-109, 1191.

[10] G. E. Karniadakis and K. S. Choi, "Mechanisms on transverse motion in turbulent wall flows," *Anual Reviews in Fluid Mechanics*, vol. 35, pp. 45-62, 2003.

[11] I. Tani, "Drag Reduction by Riblet Viewed as a Roughness Problem," Proceedings of Japanese Academy, 1988.

[12] L. Sirovich and S. Karlsson, "Turbulent Drag Reduction by Passive Means," *Nature*, vol. 388, p. 753, 1997.

[13] L. Sirovich, K. S. Ball and L. R. Keefe, "Plane waves and structures in turbulent channel flow," *Physics of Fluids*, vol. 2, pp. 2217-2226, 1990.

[14] E. R. Gowree, C. J. Atkin and S. Gruppetta, "A simple digital-optical system to improve the accuracy of hot wire measurements," *Measurement Science and Technology*, vol. 26, no. 9, 2015.

[15] F. H. Clauser, "Turbulent boundary layers in adverse pressure gradients," *Journal of Aeronautical Sciences*, vol. 21, no. 2, pp. 91-108, 1954.

[16] L. Gaudet, "Experimental Investigation of Turbulent Boundary Layer at High Reynolds Number and a Mach Number of 0.8," *Aeronautical Journal* , p. 83, 1986.

[17] J. Jimenez, S. Hoyas, M. P. Simens and Y. Mizuno, "Turbulent Boundary Layers and Channels at Moderate Reynolds Number," *Journal of Fluid Mechanics*, vol. 657, p. 335, 2010.

Author's Email Address

erwin.gowree.2@city.ac.uk

Copyright Statement